Design and Analysis of Initial High-Powered Solid Rocket Motors by Kennesaw Rocketry Team

James Carroll[1] and Gaurav Sharma[2]

Kennesaw State University, Marietta, Georgia, 30060, United States

To begin a program of student-developed solid propulsion at the Kennesaw Rocketry Team, three reloadable solid rocket motors were designed and analyzed to match performances with H100, J250, and K535 commercial motors from Aerotech Consumer Aerospace. Each motor utilizes an established pre-developed formula of Ammonium Perchlorate Composite Propellant and BATES grain geometries to achieve similar thrust, total impulse, burn time, and dimensions while allowing for multiple test firings. Performance predictions were found using OpenMotor and ProPEP 3 software programs and validated with hand calculations to achieve a 1-5% deviation from the commercial motors' performances. Structural and thermal predictions for each motor's case, liner, forward closure, nozzle, and bolt retention were found with hand calculations and validated with Finite Element Analysis simulations in the software program Ansys. Factors of safety ranged from 1.5 in replaceable components to well above 5 in critical reusable hardware for both mechanical and thermal stresses. Results have created three designs that can perform at least 5 test firings with significant safety margins and low costs to provide a foundation for future propulsion efforts of the Kennesaw Rocketry Team.

I. Introduction

The Kennesaw Rocketry Team (KRT) was revived in 2023 and has grown to become a premier competition team on campus with 30+ student members. KRT's ultimate goal is to achieve a spaceshot with custom structures, recovery, avionics, and propulsion systems of which propulsion is the least researched and developed. To address this, KRT began the propulsion subteam for the 2025-2026 academic year to begin hands-on research and development of solid rocket motors. Due to the team's infancy and relatively low budget, a project was undertaken to design and simulate three reloadable solid rocket motors based on commercial products with goals of simplicity, comparable performance, and cost-effectiveness. Each motor was designed to handle at least 5 test firings without significant wear or damage and be able to fit within typical high-powered rockets. The commercial products chosen were the Aerotech H100, J250, and K535 Disposable Motor Systems (DMS). SolidWorks models of the team designed motors are shown in the figure below with units in millimeters:

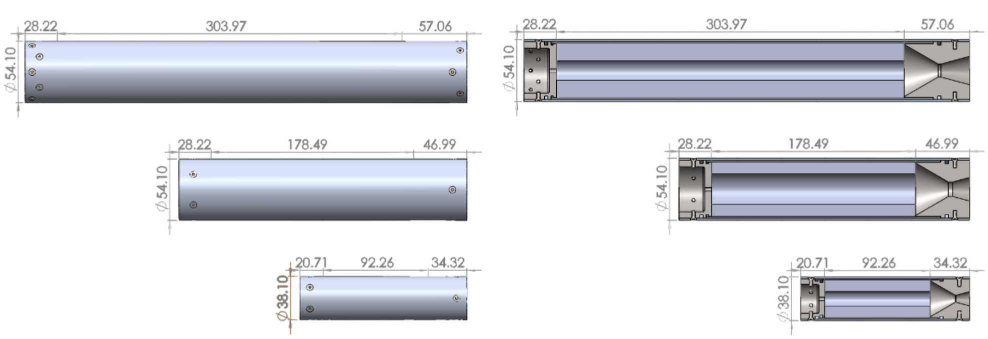

Fig. 1 CAD Models of KRT Designed H100 (Bottom), J250 (Middle), K535 (Top)

[1] Undergraduate Student, Kennesaw State University, AIAA Student Member 1549890

[2] Professor, Kennesaw State University, AIAA Senior Member

The decision to design the motors as reloadable instead of disposable systems is to save costs as each motor can handle multiple test batches. This paper documents the process of design considerations and analysis for this project to both educate future propulsion members and provide a template for small-scale solid motor designs.

II. Propellant Simulation

A. Fundamental Theory

The first step to developing solid motors is understanding the fundamental chemistry and physics which govern their performance and properties. Like most amateur solid motors, the selected propellant used for this project uses ammonium perchlorate as an oxidizer, aluminum powder as a fuel, hydroxyl-terminated polybutadiene (HTPB) as a binder, and an isocyanate compound as a curative. Known as Ammonium Perchlorate Composite Propellant (APCP), this type of solid propellant is widely used for its relative safety and ease of manufacturing [1]. The fundamental goal of any solid motor is to provide sufficient thrust to a vehicle, which is accomplished by turning the solid APCP into high velocity gas exiting from the nozzle thus producing thrust. The equation of thrust is given as:

$$F = \dot{m}v_e + (P_e - P_a)A_e \tag{1}$$

where $\dot{m}$ is mass flow rate, v_e is the velocity of the exhaust gas, P_e is the pressure at the nozzle exit, P_a is the ambient pressure, and A_e is the area of the nozzle's exit. Since each motor will have optimized nozzles fired at sea level, the $(P_e - P_a)A_e$ term can be neglected and the $\dot{m}v_e$ term focused on. The equations for mass flow rate $\dot{m}$ and exhaust velocity v_e are:

$$\dot{m} = A_b r \rho_b \tag{2}$$

$$v_e = \sqrt{2T_0\left(\frac{R'}{m}\right)\left(\frac{\gamma}{\gamma-1}\right)\left[1 - \left(\frac{p_e}{p_0}\right)^{\left(\frac{\gamma-1}{\gamma}\right)}\right]} \tag{3}$$

where A_b is the area of the burning surface, r is the burn rate of the propellant, ρ_b is mass density, T_0 is the chamber temperature, R' is the universal gas constant, m is the molecular weight of the propellant, γ is the specific heat ratio of the propellant, and P_0 is the chamber pressure. The equation for burn rate r is given as:

$$r = aP_c^{\,n} \tag{4}$$

where a is the burn rate coefficient, P_c is the chamber pressure, and n is the burn exponent. Typically, the a and n values can be only found through a motor test campaign [3]. However, since a pre-developed formula is utilized the burn rate can be known at any moment given the chamber pressure. From Eqn. 2 and Eqn. 3, by optimizing the chamber pressure of each motor with a known nozzle throat size, the maximum burn rate, velocity of exhaust gases, and mass flow will be achieved thus giving the highest possible thrust. To achieve the optimal chamber pressure, the optimal nozzle expansion ratio must be found which shall be discussed in later sections.

B. Propellant Selection

The process of creating a unique propellant formula is a long, difficult, and potentially dangerous process that KRT is not eager to undertake for this project. Instead, using a pre-developed formula with known characteristics will greatly reduce development time and costs. Developed by the MIT rocket team, "Cherry Limeade" is a widely used formula for those new to solid propellant with well documented properties. The specific formula used by KRT is the originally published version, but variations of the formula can be found online such as the MIT Rocket Team Wiki. Below are tables detailing the Cherry Limeade formula used and published propellant data provided by the MIT Rocket Team:

Table 1 Cherry Limeade Propellant Formula

Ingredient	HTPB	MDI	Castor Oil	PDMS	Triton X100	30μ Aluminum	200μ Ammonium Perchlorate	90μ Ammonium Perchlorate
Percentage, %	14.89	2.21	0.30	0.05	0.05	7.50	65.50	9.50

Table 2 Cherry Limeade Propellant Values

Property	Specific Impulse, s	Density, kg/m^3	Burn Coefficient, mm/s	Burn Exponent	Specific Heat Ratio	Price Per Weight, $USD/kg
Nominal Value	227	1688	0.6346	0.3274	1.21	26.87

An important concept to understand when using a pre-developed propellant formula is understanding its optimal Kn range. Kn is the ratio between a motor grain's burning surface area to the nozzle's throat, which gives a useful unitless number to ensure the motor burns efficiently and simulations will be accurate. Cherry Limeade is recommended to operate within a Kn range of 180-250 for best results [3].

C. Geometry Selection

Another consideration faced in solid propellant design is the patterns used within the grain's cores. By changing the pattern used, thus changing how much propellant area is being burned at any given time, the thrust-curve profile, operating pressure, and burn time of the motor can be modified to better suit desired performance. Common grain geometries used in amateur rocketry include tubular/BATES, finocyl, star, and moon burners [4]. KRT has chosen BATES grain geometry due to its ease of manufacturing, reliability, and widespread use in solid motor testing. A single propellant pour will be bonded directly to the liner to create a single cylindrical core with the ends of the grain free to burn. The method is sometimes called a core burning or progressive BATES configuration. Due to the long singular grain and uninhibited ends each motor, the BATES geometry creates a thrust curve which is gradually increasing and roughly linear across the burn time. Since the production of these motors will be a labor-intensive process, ensuring grain geometry can be accurately replicated several times assists KRT's efforts to ensure consistency in performance and safety. A cylindrical shape simplifies manufacturing techniques needed to create the necessary geometry, such as the propellant poured around a metal rod with mold release. Since these motors will be relatively small with short burn times, the increasing temperature and pressure created from the BATES geometry still leaves large factors of safety that ensure the motor is unlikely to experience any structural failures.

D. Performance Simulations

As stated before, one of the major goals of this project is to have KRT's motors achieve similar performance to commercially available products. The specific parameters being targeted in motor performance are same motor designation, similar average thrust, similar total impulse, similar burn time, similar propellant mass, and similar motor length. Due to the vast range of formulas and equations used in solid propellant design and performance calculations, it is highly advantageous to utilize software to expedite the process. KRT has decided to utilize the free and open-source software program OpenMotor for propellant simulations and sizing of each motor's grain and core dimensions. The general approach to this process was to create a rough estimate of grain and core sizes using phenolic liner dimensions, then defining the nozzle converging and throat dimensions to target a mass flux under 4006 kg/m^{2}s, a grain port to nozzle throat ratio of at least 2, and a Kn range between 150-275. Afterwards, the grain and core sizes are refined to achieve the target parameters, with final nozzle sizing done using the optimum expansion ratio.

Revisiting Eqn. 1, 2, and 3 it is now possible to evaluate the mass flow, gas exhaust velocity, and thrust. Using the collected data and average pressure of each motor, the following table was calculated:

Table 3 Motor Thrust and Percent Difference Calculations

Thrust Calculation	v_e, m/s	ṁ, kg/s	Average Thrust, N	Total Impulse, Ns	% Difference to OpenMotor	% Difference to Aerotech Motor
H100	2190.13	0.046	100.75	238.78	1.27	2.02
J250	2049.91	0.127	260.34	718.54	2.66	0.35
K535	2203.52	.237	522.23	1504.04	3.50	4.77

Each motor's theoretical thrust is within the range of values given by OpenMotor simulations as well as the commercial Aerotech product each motor is based on. The OpenMotor difference can be explained by the software simulating additional factors such as slag buildup, corrosive burning, and unburned propellant into its simulations that change performance. Additionally, it should be noted that the difference between theory and simulation increases with motor size. These results indicate that as motors become larger, the difference in calculation to simulation will become larger unless care is taken to ensure each calculation and simulation is set up and applied correctly. The Aerotech differences can be explained by the company's motors using different propellant formulas, thus having differing specific heat ratios and chamber pressures.

For later simulations, it is important to understand the temperature being faced by each component. Using the free software program ProPEP 3 and inputting the propellant formula and chamber pressure, the calculated chamber temperature in each motor is 2778.31K for the H100, 2766.19K for the J250, and 2778.21K for the K535. To find the stagnation temperature T_t for a specific location in the motor nozzle the following equation can be used:

$$T_t = \frac{T_c}{\left(1 + \frac{\gamma - 1}{2} M^2\right)} \tag{5}$$

where T_c is the chamber temperature and M is Mach number at the location. One way Mach number can be found is by the equation:

$$\frac{A}{A^*} = \frac{1}{M}\left(\frac{1 + \frac{\gamma - 1}{2} M^2}{1 + \frac{\gamma - 1}{2}}\right)^{\frac{\gamma+1}{2(\gamma-1)}} \tag{6}$$

where A is the cross-sectional area of the specific location and A^* is the area of the nozzle throat which forms the area ratio A/A^*. This equation cannot be algebraically rearranged to find M directly, but a graph of Eqn. 6 can be made to estimate Mach number from the area ratio, then a graph of Eqn. 5 can be plotted to find temperature [5]. The following graphs plot the area ratio on the y-axis and Mach number on the x-axis, then the temperature in kelvin on the y-axis in a logarithmic scale and Mach number on the x-axis:

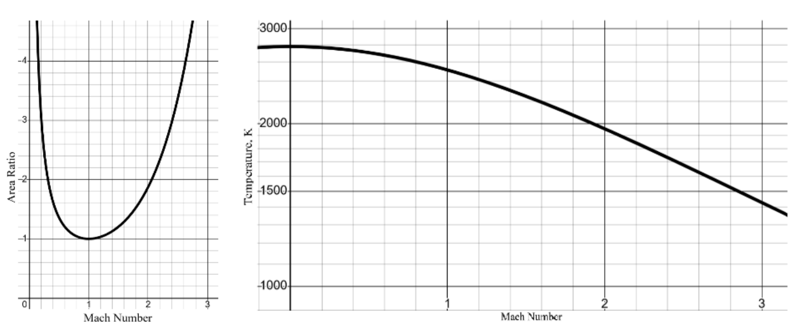

Fig. 2 Area Ratio vs. Mach Number (Left) and Stagnation Temperature vs. Mach Number (Right)

The nozzles' converging sections experience temperatures close to chamber temperatures from 2800-2550K, the throats see roughly 2550-2500K, and the nozzles' diverging sections can see temperatures around 2500-1500K. The results of these graphs gave useful data to assist in material selection for the liners and nozzles.

III. Structural Components Design and Analysis

Reloadable motors typically come in 6-7 major components including the liner, forward closure, aft closure, nozzle, O-rings, case, and propellant. Due to the retention system KRT utilized discussed in later sections, the need for an aft closure was unnecessary. O-rings were not a significant enough component to warrant its own section but are discussed as needed. Larger amateur motors typically use a Head End Ignition (HEI) bolt threaded through the top of the motor to quickly ignite the propellant but was deemed unnecessary for this project as the motors are small enough to be lit with commercial products. Additionally, a pressure transducer could not be placed through the forward enclosure if an HEI bolt was present due to the small diameter of the motors. The following sections detail design considerations, justifications, and structural and thermal analysis for each major component.

A. Liners and Cases

The purpose of the liner within a solid motor is to provide thermal protection from the hot gases as the propellant burns, as well as assist in containing the chamber pressure. The purpose of the case is to hold all components together and withstand the various stresses during a burn. The motors will use commercially available phenolic liners which are composite materials created by winding layers of paper infused with phenolic resin together to create strong and stiff material with excellent heating properties. The cases will be machined by KRT from commercially available aluminum 6061-T6 round tubes. 6061-T6 aluminum was chosen due to its widespread availability, low cost, ease of machining, and acceptable mechanical and thermal properties for this project.

The principal stress considerations for the liners and cases are axial stress parallel to the central axis and hoop stress perpendicular to the central axis. Hand calculations for these values are rather simple if the component can be considered a thin-walled pressure vessel, but the team deemed it beneficial to confirm calculated values with simulation data as well as to hone member analysis skills for future projects. A component is assumed to have equal forces acting on all its entire radial surface if the ratio of diameter to thickness, or D/t value, is greater than 20. For the H100, the D/t value for the liner is 34.93mm/0.80mm or 43.66 and the value of the case is 38.10mm/1.48mm or 25.74. For both the J250 and K535, the D/t value of the liners is 50.34mm/1.36mm or 37.02 and the value for the cases is 54.10mm/1.76mm or 30.74. Since all the values are above 20, the simpler equations can be applied. The equation for hoop stress is given as:

$$\sigma_h = \frac{pD}{2t} \tag{7}$$

where p is the pressure, D is the diameter of the pressure vessel, and t is the thickness of the vessel. This equation can be rearranged to find the maximum possible pressure the case and liner can handle:

$$p = \frac{2\sigma_h t}{D} \tag{8}$$

When finding the maximum pressure, especially for ductile materials, the tensile yield strength of the material should be used. The equations for longitudinal stress and maximum pressure are the same as Eqn. 7 and 8, simply with the 2 replaced by a 4. It is important to observe that hoop stress is the primary concern as longitudinal stress will always experience half the stress and contain double the maximum pressure compared to radial stress. For this reason, only the hoop stress equations will be used to calculate stress and maximum pressure. For each calculation, chamber pressure is increased by 10% to account for propellant imperfections. From the above information, a table of variables and calculations was created:

Table 4 Stress Variables and Calculated Values of Motors

Variable/ Calculation	Diameter, m	Thickness, m	Chamber Pressure, MPa	Tensile Yield Strength, MPa	Hoop Stress, MPa	Maximum Pressure, MPa	Factor of Safety
H100 Liner	0.035	0.0008	3.31	140	72.40	6.40	1.93
H100 Case	0.038	0.0015	3.31	276	41.93	21.79	6.58
J250 Liner	0.050	0.0014	2.05	140	36.61	7.84	3.82
J250 Case	0.054	0.0018	2.05	276	30.75	18.40	8.98
K535 Liner	0.050	0.0014	5.26	140	93.93	7.84	1.50
K535 Case	0.054	0.0018	5.26	276	78.90	18.40	3.50

For each case the desired factor of safety was a minimum of 3 which was achieved for all three motors. Having such high factors of safety not only ensures a much lower chance of any failures but ensures the motor case can be fired many times with confidence in its structural integrity. For each liner, the minimum factor of safety was 1.25 which was met with acceptable results but were noticeably lower than the cases. The reason for the lower standard is because liners are primarily meant for thermal protection and are discarded after each firing. Some deem it unnecessary to calculate stress on the liners for these reasons, but they are calculated and discussed here as it is important to ensure the liners will neither deform nor crack during each firing.

To confirm these calculations, a static structural simulation was created in Ansys Mechanical. Only cases were simulated for abbreviation and due to the excellent results. Additionally, a transient thermal analysis was conducted on the liner and case with convection and radiation applied on the inner surface with a film coefficient value of 0.2 W/mK for phenolic over the respective burn time of each motor. Ablative materials like phenolic can be difficult to simulate as they erode over the period of the burn. To simplify the analysis, the phenolic char layer emissivity of 0.05 is applied for radiation as it affects the inner surface of the material:

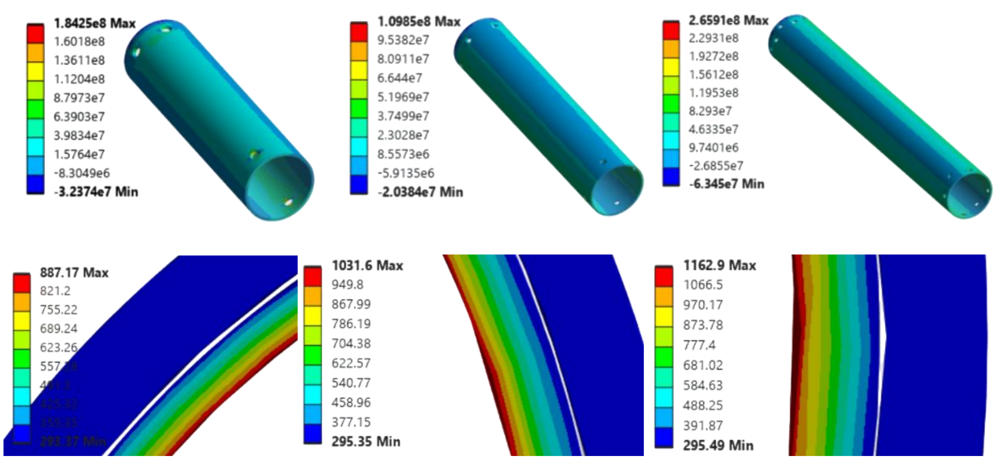

Fig. 3 Stress and Thermal Analysis of H100 (Left), J250 (Middle), and K535 (Right) Case and Liner

When a cross section of the H100 model was taken, the highest radial stress found on the inner wall was 41.30MPa and the highest axial stress found was 20.76MPa, giving percent differences of 1.51% and 0.98% respectively. For the J250, the radial stress was 30.56MPa and axial stress was 15.43MPa for percentage differences of 0.62% and 0.36% respectively. For the K535, the radial stress was 78.15MPa and axial stress was 39.35MPa for percentage differences of 0.96% and 0.25% respectively. These values, being very close to the calculated values, give KRT confidence in the structural integrity of these liners and cases.

For detail, the thermal simulation images used zoomed-in cross sections of the case and liner at the location of highest temperature. The gap seen within the picture reflects real-life dimensions, however contacts were used in the simulations to give results as if the case and liner were directly touching. From the thermal simulation, the inner surface of the case should not exceed 303.95K, 307.25K, and 311.71K. Aluminum 6061-T6 can reach temperatures of 477K without losing significant strength and begins to melt at 855.15K [6], giving factors of safety of 1.57, 1.55, and 1.53 as well as 2.81, 2.78, and 2.74 respectively. Additionally, the short-term temperature the phenolic char layer can handle is 1273.15K [7] giving factors of safety of 1.44, 1.23, and 1.10 respectively. These factors of safety may cause concern; however, it is important to note that this simulation assumes that convection and radiation is directly applied to the walls for the entire burn and does not consider the char layer ablating away any heat from the motor. Since these simulations are worst-case scenarios for each motor yet still have factors of safety above 1, these results help affirm that each motor will handle the thermal and mechanical stresses across multiple firings.

B. Forward Closures

The purpose of the forward closure is to contain the pressure of the motor in the upper sections of the motor and provide space for ignition bolts, pressure sensors, motor retention and ejection charges, etc. KRT has decided to manufacture all forward closures from 304 stainless steel round bars due to its more desirable thermal properties. Each forward closure features two different sized O-rings with the smaller sitting within the phenolic liner for redundancy and preventing any gas reaching between the liner and case. Additionally, each forward closure will have a 1/8-inch NPT threaded hole in the center to allow for a pressure transducer during test firings. For future flight-ready motors, the threaded hole will either be replaced with a receiver for a threaded rod, or a lip will be machined onto the nozzle.

To keep each motor as simple as possible, the forward closure was designed without a thermal protective layer as it would need replacement after each firing. With chamber temperatures around 2800K, stainless steel can begin to fail; however, it can withstand high temperatures for short periods of time with no loss of strength. A transient thermal analysis was conducted in Ansys Mechanical with convection and radiation applied to the bottom of the closure with a film coefficient of 16.2 W/mK and emissivity of 0.2 for the respective burn times. Additionally, a static structural analysis was conducted with chamber pressures applied to the bottom of each closure with fixed supports at each bolt hole:

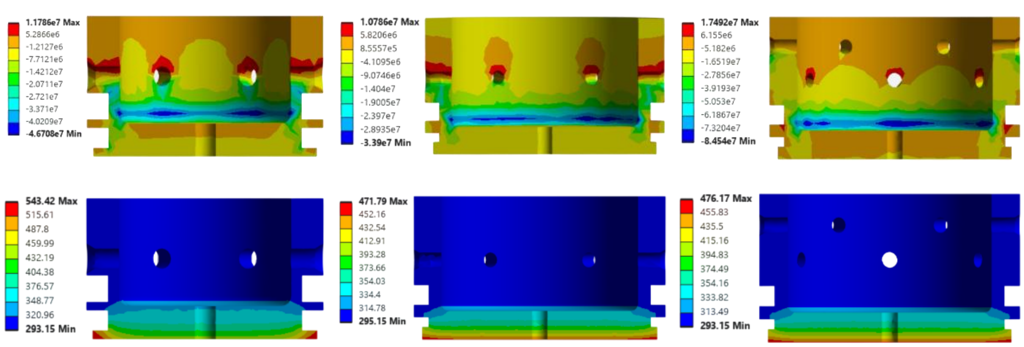

Fig. 4 Stress and Thermal Analysis of H100 (Left), J250 (Middle), and K535 (Right) Forward Closure

The stress and thermal simulations show results that are in-line with calculations discussed in later sections and fall well below the stress necessary to damage or deform the forward closures. With burn times all below 3 seconds, the high chamber temperatures don't have enough time to transfer into the stainless steel and cause any deformation or diminish strength. 304 Stainless steel has a maximum short-term operating temperature of 1143.15K and a solidus point of 1673.15K [6] giving a factor of safety of 2.10, 2.42, 2.40 respectively before any strength is lost and a factor of safety of 3.08, 3.55, 3.51 respectively before the closure begins to melt. Additionally, the high-temperature silicon rubber O-rings have higher operating temperatures than the temperatures seen on either groove.

C. Nozzles

The purpose of the nozzle is to funnel and accelerate the gases in the chamber to reach Mach velocity at the throat, then rapidly expand and reach maximum velocity at the nozzle's exit. KRT has decided to machine the nozzle from 304 stainless steel round bars due to its acceptable thermal properties. Graphite was initially considered for its excellent thermal resistance, however the machining of graphite releases dust which is extremely harmful to personal health and machine operations. Since the nozzle will be made by machines owned by the university, graphite was considered undesirable [8]. For future larger motors, some graphite such as a graphite throat will likely be necessary. There are multiple ways to approach the design of a nozzle, but KRT began by constraining each nozzle's converging section to a 30° half-angle and diverting section to a 15° half-angle for ease of machinability. The throat was then sized for port-to-throat ratio of above 2 and for acceptable pressure and performance before the nozzle was optimized for best performance. As mentioned previously, to achieve the highest possible thrust the nozzle must be optimally expanded so that the exhaust gas at the very end of the nozzle matches the pressure of the surrounding atmosphere. The area of the exit diameter A_e can be found by:

$$A_e = \frac{A^*}{(\frac{\gamma+1}{2})^{\frac{1}{\gamma-1}}\left(\frac{P_e}{P_0}\right)^{\frac{1}{\gamma}}\sqrt{\left(\frac{\gamma+1}{\gamma-1}\right)\left[1-\left(\frac{P_e}{P_0}\right)^{\frac{\gamma-1}{\gamma}}\right]}} \tag{9}$$

From the cross-sectional area formula, the exit diameter D_e can be derived as:

$$D_e = \sqrt{\frac{4A_e}{\pi}} \tag{10}$$

Using the average chamber pressure of 2.51MPa and throat diameter of 6.096mm, the optimal exit diameter of the H100 is 12.43mm. With an average pressure of 1.54MPa and throat diameter of 12.7mm, the optimal exit diameter for the J250 is 21.85mm. With an average pressure of 3.41MPa and a throat diameter of 11.43mm, the optimal K535 exit diameter is 26.07mm.

A static structural analysis was conducted with chamber pressures applied to the top and converging section of each nozzle with fixed support at each bolt hole. Additionally, a transient thermal analysis was conducted in Ansys Mechanical with convection and radiation applied to the inside faces of the nozzle with a film coefficient of 16.2 W/mK and emissivity of 0.2 for the respective burn times. The temperatures applied to each nozzle's converging, diverging, and throat section was based on conservative estimations from Eqn. 5 and 6 and Fig. 3. Each nozzle section had 2 separate temperatures applied for more accurate results:

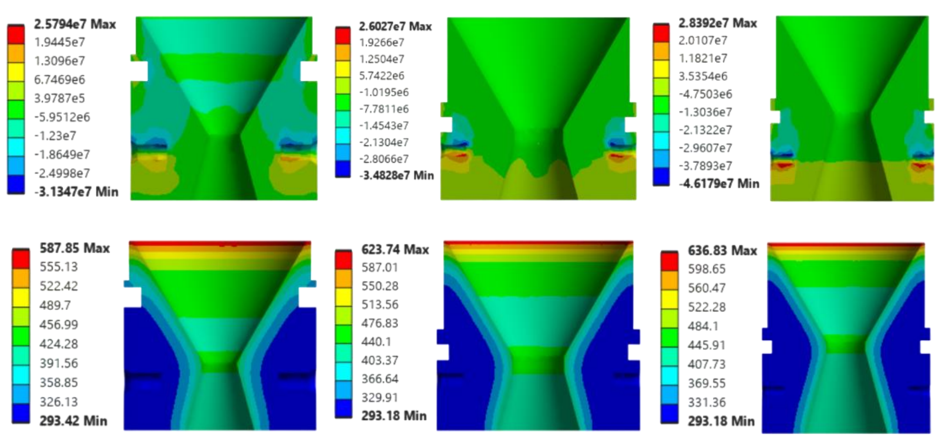

Fig. 5 Stress and Thermal Analysis of H100 (Left), J250 (Middle), and K535 (Right) Nozzle

The stress simulations results are in line with their expected values and leave plenty of factors of safety for both the nozzles and bolts; There should be no damage or deformation to the nozzles across all the burns. The thermal analysis gave results slightly higher than expected but can be explained by using a limited number of convection and radiation data points. Even with this conservative estimate, there is still a factor of safety of 1.95, 1.83, and 1.80 respectively before any significant loss in strength and a factor of safety of 2.85, 2.68, and 2.63 respectively before the nozzle begins to melt. All O-rings and bolts in the thermal analysis will see practically no increase in temperature across the short burn times of each motor. These excellent results give KRT reason to believe that each motor could perform all burns with no issue. However, due to factors like slag buildup and corrosion of the stainless steel that could affect performance or thermal properties, 2-3 nozzles will be made for each motor, and each nozzle will be inspected after each firing to ensure safety.

D. Retention

Typical retention methods amateur solid motors utilize are snap rings, pins, and bolts. KRT has chosen to use 10.9 grade alloy steel M3 8-millimeter-long countersunk flat head bolts to simplify design, manufacturing, and simulation. The choice of bolts instead of pins or snap rings was made as they are widely available for low cost and have proven to be completely sufficient for this project. This method allows KRT to forgo an aft closure and instead drill holes within the nozzle itself to contain the pressures of the motor. This additionally simplifies manufacturing by only requiring simple radial hole patterns, a countersink, and tapping bit which allows the bolts to sit flush within the case for potential use in a rocket's motor mount. As KRT will be using school-owned machines, it is important that the design has high manufacturing robustness to account for any misalignments or human error. The principal stress considerations involving bolts are bolt shear which is the shear force at which the bolt itself breaks, bolt tear out which is the force required to tear a bolt from the material it is screwed into, and hole bearing failure which is the force at which the bolt causes deformation in the material. The failure force F_b of a bolt can be found with the following equation:

$$F_b = n\left(\frac{\pi}{4}D^2\right)\sigma_{bolt} \tag{11}$$

where n is the number of shear planes, D is the diameter of the bolt, and σ_{bolt} is the ultimate shear strength of the bolt. Since only the interaction of the bolt between the case and closure/nozzle is considered, n can be set as 1. To generate a conservative estimate, the minor bolt diameter of 2.46mm and lower range of ultimate shear strength of 620 MPa can be used [6]. Plugging the values into Eqn. 11, a bolt shear failure force of 2946.7N is determined. To find the shear force that acts on the bolt, the shear force of the forward closure/nozzle and the axial stress of the case will be combined. The force on the forward closure/nozzle can be calculated by using the inner diameter of the case to find the area, then multiplying by the chamber pressure. The force on the case can be found by using the thickness to find area of the case cross section, then multiplying by the axial stress found by halving the hoop stress. By using values found in table 4, the following table was calculated:

Table 5 Calculations of Bolt Shear Forces

Variable/ Calculation	Axial Shear Force, N	F. Closure/Nozzle Shear Force, N	Total Shear Force, N	# of bolts	Factor of Safety
H100 F. Closure	148.19	3184.50	3332.69	6	5.31
H100 Nozzle	148.19	3184.50	3332.69	4	3.54
J250 F. Closure	156.50	4089.71	4246.21	6	4.16
J250 Nozzle	156.50	4089.71	4246.21	4	2.78
K535 F. Closure	401.54	10493.59	10895.13	12	3.26
K535 Nozzle	401.54	10493.59	10895.13	8	2.16

The number of bolts necessary to maintain a factor of safety of 2 or more was determined using the calculated total shear force and the bolt shear failure force. The K535 required significantly more bolts than the H100 or J250 due to the relatively high chamber pressure. If compared to the factors of safety in table 4, it should be noted that the cases' factors of safety are consistently higher and have a higher minimum compared to the factors for the closures and nozzles. This was a deliberate choice to ensure that the first component to fail would be the nozzle, followed by the forward closure. The case exploding is the most dangerous failure possible which can send bits of hot metal, phenolic, and propellant in every direction. However, if the nozzle is likely to fail first with the forward closure to follow, the damage can be somewhat controlled and minimized as the pressure and temperature of the motor will rapidly fall without either component [9]. When evaluating the factors of safety it is important to remember these are calculated with conservative estimates that assume an unideal scenario. Bolt tear out F_{to} can be calculated with the following equation:

$$F_{to} = 2bt\sigma_c \tag{12}$$

where b is the distance from the center of the bolt to the case's edge, t is the thickness, and σ_c is the ultimate shear strength of the material. Using the ultimate shear strength of aluminum 6061-T6 of 207MPa, a safe shear strength estimate for 304 stainless steel of 450MPa [6], and b and t values from the SolidWorks models, the necessary values can be calculated. For components with multiple rows of radial holes such as the K535, the value of b is taken as the average of the two rows' distance from the edge. Bolt bearing failure F_{bf} can be found using the equation:

$$F_{bf} = dt\sigma_{bs} \tag{13}$$

where d is the diameter of the bolt, t is the thickness of the case material, and σ_{bs} is the bearing yield strength of the material. This equation assumes that the diameter of the bolt is the same as the hole, however this cannot be counted on as the real bolt will only be in contact with a fraction of the hole. A useful rule of thumb for a safe estimate is to replace the d and t term by dividing the area of the major hole by 4, which gives a value of 7.07e-6 m^2. Using the bearing yield strength of Aluminum 6061-T6 of 386 MPa and a safe estimate for 304 stainless steel of 500 MPa [6], the necessary values can be calculated. For each component it is also assumed to be taking the entire force of the motor as shown in table 5. Below is the table of calculated values for bolt tear out F_{to} and bolt bearing failure F_{bf} :

Table 6 Calculations for Bolt Tear Out and Bearing Failure

Variable/ Calculation	b, m	t, m	F_{to}, N	F_{bf}, N	Force on Component, N	# of bolts	F_{to} Factor of Safety	F_{bf} Factor of Safety
H100 Case	0.0089	0.0015	5526.90	2729.02	3332.69	6/4	9.95/6.63	4.91/3.28
H100 F. Closure	0.0089	0.0048	38448.00	3535.00	3332.69	6	69.22	6.36
H100 Nozzle	0.0089	0.0068	54468.00	3535.00	3332.69	4	65.37	4.24
J250 Case	0.0130	0.0018	9687.60	2729.02	4246.21	6/4	13.69/9.12	3.86/2.57
J250 F. Closure	0.0130	0.0055	64350.00	3535.00	4246.21	6	90.93	5.00
J250 Nozzle	0.0130	0.0065	76050.00	3535.00	4246.21	4	71.64	3.33
K535 Case	0.0094	0.0018	6967.62	2729.02	10895.13	12/8	7.67/5.12	3.01/2.00
K535 F. Closure	0.0094	0.0055	46530.00	3535.00	10895.13	12	51.24	3.89
K535 Nozzle	0.0094	0.0065	54990.00	3535.00	10895.13	8	40.34	2.60

Evaluating table 5 and 6, the factor of safety for bolt tear out is consistently higher than the bolt shear safety factors. This means that the bolts will be more likely to break apart before tearing through the material they are holding onto. This is another deliberate safety design to minimize damage to the case, forward closure, or nozzle in the event of failure. When the bearing stress is examined, every factor of safety has a minimum of 2 with the vast majority having a factor of at least 3. This gives KRT confidence that no component will experience significant fatigue or deformation during its service lifetime.

To confirm the calculations above, a static structural analysis was performed in Ansys Mechanical. For the sake of brevity, only the bolts that are held in the K535 case and nozzle were simulated as it has the lowest factor of safety. A force of 10895.13N was applied to the nozzle with the case acting a fixed support:

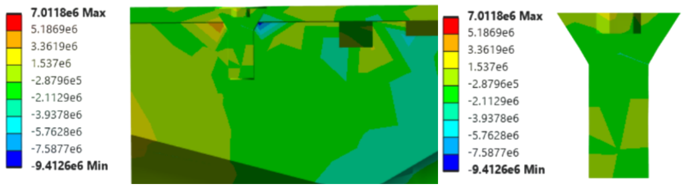

Fig. 6 Stress Analysis of M3 Bolt Under Test Load

The results fall within line of what was expected from the above calculations. From the stresses shown, no bolt should experience more than 7.02MPa when the ultimate shear strength is 620MPa giving plenty of safety across each motor.

IV. Conclusion

As stated in the introduction, the purpose of this project was to design and simulate 3 solid rocket motors that can withstand 5 test fires each while achieving similar performance and size to commercially available products. KRT has concluded that all goals have been achieved handily and feel ready to move into manufacturing, test firings, and designing larger motors for future use. In a cost analysis performed by KRT it was found that the average batch costs for each motor were just \$3.05, \$9.75, and \$21.09 for a total propellant cost of \$169.45. KRT estimates that costs for motor hardware, safety equipment, test stand materials, and additional propellant test batches should not exceed \$4000 with costs easily lowered by borrowing equipment, purchasing alternate materials, etc.

Acknowledgments

KRT would like to give special thanks to the team's mentor Allen Isdell for his guidance and support in all KRT efforts. KRT would also like to acknowledge Jorge Blanco of Southern Area Rocketry for his support of this project and suggestion to base each motor off a commercially available product.

References

[1] Sutton, G. P., and Biblarz, O., *Rocket Propulsion Elements*, 9th ed., Wiley., New Jersey, 2017, Chaps. 3, 12, 13 ,15.

[2] Meier, A., (2024 December 9)., *Solid Propulsion Subteam*., MIT Rocket Team Wiki, wikis.mit.edu/confluence/display/RocketTeam/Solid+Propulsion+Subteam

[3] McBride, F. J., "Exploring in Aerospace Rocketry: 6. Solid-Propellant Rocket Systems," NASA TM-52393, 1967

[4] Nakka, R., (2023, March 23)., *Solid Rocket Motor Theory Index Page*., Richard Nakka's Experimental Rocketry Web Site, www.nakka-rocketry.net/rtheory.html

[5] Connor, F. J., "Exploring in Aerospace Rocketry: 2. Propulsion Fundamentals," NASA TM-52389, 1967

[6] ASM Handbook - *Properties and Selection: Nonferrous Alloys and Special Purpose Materials*, 10th ed., Vol. 2, ASM International, 1990. https://doi.org/10.31399/asm.hb.v02.9781627081627

[7] "RCS Phenolic Tubing Specifications," RCS Rocket Motor Components, Inc., 2023

[8] Stevenson, J., "Design of Nozzle for High-Powered Solid Rocket Propellant." Undergraduate *Journal of Mathematical Modeling: One + Two*, Vol. 9, No. 2, 2018 https://doi.org/10.5038/2326-3652.9.1.4895

[9] Patel, J., Patil, Y. M., and Gelot, N. B., "Analytical and Numerical Study of Mechanical Behaviour of Bolted Joints –A Review," *International Journal of Advanced Research in Science, Communication and Technology*, Vol. 3, No. 5, DOI: 10.48175/IJARSCT-11698